The Canadian Mineralogist
Vol. 37, pp. 711-720 (1999)

CRYSTAL STRUCTURES OF NEAR-END-MEMBER PHLOGOPITE AT HIGH TEMPERATURES AND HEAT-TREATED Fe-RICH PHLOGOPITE: THE INFLUENCE OF THE O,OH,F SITE

RONALD L. RUSSELL AND STEPHEN GUGGENHEIM§

Department of Earth and Environmental Sciences, University of Illinois at Chicago, 845 W. Taylor Street, Chicago, Illinois 60607, U.S.A.

ABSTRACT

The crystal structure of end-member phlogopite-1*M* from White Well, Australia, was determined by refinement using single-crystal X-ray data to 600°C ($R = 0.069$, $wR = 0.096$ at 600°C). Cell parameters were refined at 20, 150, and thereafter at 50°C intervals to 600°C. The rate of expansion of the metric unit-cell dimensions is linear. The expansivity of the *c* dimension is 1.81×10^{-5} °C^{-1}, and 1.40 and 1.34×10^{-5} °C^{-1} for the *a* and *b* dimensions, respectively (compared to fluorophlogopite in a previous study: 24° to 600°C, $\alpha_a = 0.86$, $\alpha_b = 0.75$, and $\alpha_c = 1.81 \times 10^{-5}$ °C^{-1}). The OH-rich octahedra (*M*1, *M*2) expand without changing shape significantly at elevated temperatures, in contrast to F-rich octahedra in fluorophlogopite, which become elongate approximately along the *c* axis. The interlayer site becomes elongate in phlogopite with increasing temperature relative to fluorophlogopite, although the site shows general flattening with increasing temperature. We also refined the room-temperature structure of a sample of Fe-rich phlogopite-1*M* sample from Silver Crater, near Bancroft, Ontario, and the same phlogopite after heat treatment at 904°C for 24 hours (untreated: $R = 0.039$, $wR = 0.043$; heat-treated: $R = 0.039$, $wR = 0.047$). In contrast to earlier studies, there was no change in Fe site occupancy from the octahedra to the tetrahedra. The octahedra (*M*1, *M*2) and the interlayer site are flattened in both the heated and unheated samples, but the heated sample shows significant flattening in all these sites over the unheated sample.

Keywords: phlogopite, heat-treated phlogopite, crystal structure.

SOMMAIRE

Nous avons déterminé la structure cristalline d'un échantillon de phlogopite-1*M* de White Well, Australie, dont la composition est proche du pôle, par affinement de données prélevées sur cristal unique jusqu'à 600°C ($R = 0.069$, $wR = 0.096$ à 600°C). Les paramètres réticulaires ont été affinés à 20, 150, et ensuite à chaque tranche de 50°C jusqu'à 600°C. Le taux d'expansion des paramètres réticulaires est linéaire. L'expansivité de la dimension *c* est 1.81×10^{-5} °C^{-1}, et celle des dimensions *a* et *b*, 1.40 and 1.34×10^{-5} °C^{-1}, respectivement (on peut comparer ces données à celles de la fluorophlogopite, déterminées antérieurement: entre 24° et 600°C, $\alpha_a = 0.86$, $\alpha_b = 0.75$, et $\alpha_c = 1.81 \times 10^{-5}$ °C^{-1}). Les octaèdres riches en OH (*M*1, *M*2) augmentent en volume sans changer de forme aux températures élevées, contrairement aux octaèdres riches en F dans la fluorophlogopite, qui deviennent allongés le long de l'axe *c*. Le site inter-feuillet devient allongé dans la phlogopite à mesure qu'augmente la température, relativement à la fluorophlogopite, quoique le site montre un applatissement général avec une augmentation en température. Nous avons aussi affiné la structure à température ambiante d'un échantillon de phlogopite-1*M* riche en Fe provenant de Silver Crater, près de Bancroft, en Ontario, et du même mica après chauffage à 904°C pour 24 heures (sans chauffage: $R = 0.039$, $wR = 0.043$; après chauffage: $R = 0.039$, $wR = 0.047$). Contrairement aux résultats antérieurs, il n'y a pas eu de changement dans l'occupation des sites par le Fe, par exemple un transfert de site octaédrique à site tétraédrique. Les octaèdres (*M*1, *M*2) et le site inter-feuillet sont applatis dans les échantillons de ce mica, chauffé ou non, mais l'échantillon chauffé montre un applatissement nettement accru à tous ces sites par rapport à l'échantillon non chauffé.

(Traduit par la Rédaction)

Mots-clés: phlogopite, phlogopite chauffé, structure cristalline.

§ *E-mail address*: xtal@uic.edu

Introduction

The storage of hydrogen and H_2O in the Earth's upper mantle occurs in silicate minerals such as phlogopite, and the serpentines, amphiboles, and possibly in some nominally anhydrous minerals (Prewitt & Finger 1992). Phlogopite, serpentines, and amphiboles, commonly occurring to depths of about 200 km before decomposition, are important because they control the introduction of H_2O into the mantle; H_2O strongly affects melting conditions and other properties of mantle material. The previous high-temperature structural study on phlogopite (Takeda & Morosin 1975) involved a synthetic fluorophlogopite. This study was the first high-temperature, single-crystal structural study of a phyllosilicate. The authors successfully related a geometric model to the observed expansion of the component parts of the structure, *i.e.*, the tetrahedral and octahedral sheets and the interlayer region. However, in terms of understanding temperature effects on phlogopite common to the Earth's upper mantle, a more hydroxyl-rich composition is appropriate. A structural study of a near end-member phlogopite allows an easy comparison to fluorophlogopite, and the effect of intermediate compositions can be readily surmised.

In contrast, interest in the effect of temperature for samples on the phlogopite–annite join generally relates to metamorphic processes, since metamorphic rocks commonly contain iron, although the importance of Fe in the Earth's mantle has been advocated by some (*e.g.*, Hazen *et al.* 1992, Anderson 1979). However, the effect of temperature on the mica structure characterized by either the presence or absence of iron also is an important crystal-chemical problem. This problem can be better understood if a comparison is made between two samples with similar structures, such as phlogopite and Fe-rich phlogopite. Most noteworthy is the ability of the Fe-rich structure to compensate for oxidation or reduction by hydrogenation or dehydrogenation. This occurs at the same site as OH–F substitution.

However, complications arising from the multiple oxidation states of iron and hydrogenation or dehydrogenation that occurs with oxidation or reduction make a high-temperature structural study of Fe-rich phlogopite difficult. Indeed, determining oxidation states by X-ray techniques is difficult and is most readily accomplished, although imperfectly, by examining bond distances. Alternatively, Mössbauer analysis gives a more precise determination of oxidation state. However, Rancourt (1994) and Rancourt *et al.* (1994) showed that differences in iron population at $M(1)$ and $M(2)$ sites of 2:1 layer silicates cannot be resolved with the Mössbauer method and that quadrupole splitting distributions result from a variety of structural and chemical features, such as Fe–F interactions (*e.g.*, Mason 1992, Rancourt *et al.* 1996).

In a structural study comparing two polytypes of Fe-rich phlogopite (previously referred to as "biotite") from Ruiz Peak, New Mexico, Takeda & Ross (1975) examined Fe-rich phlogopite-1*M* and Fe-rich phlogopite-$2M_1$ after passing hydrogen gas at 700°C over the sample to produce a reduced and hydrogenated product. Later, Ohta *et al.* (1982) used material from the same locality, but treated with hot argon gas, to produce a hydrogen-depleted and oxidized ("oxy-mica") counterpart of each polytype for comparison. This study showed that interlayer separation increases significantly with the addition of H due to electrostatic interactions (repulsions) between the interlayer cation and the H, in addition to cell-parameter expansion caused by the larger ferrous-iron cation in the reduced iron phase.

The present paper presents an *in situ* high-temperature structural study of near-end-member phlogopite. In addition, we examine, at room temperature, an iron-rich phlogopite and the same phlogopite after heat treatment. The samples of Fe-rich phlogopite were examined previously by Mössbauer spectroscopy (Rancourt *et al.* 1993).

Experimental

Samples

Phlogopite from White Well, Australia (Western Australian Museum #MDC4985), has a structural formula based on wet-chemistry techniques (Pryce 1973) of $(K_{0.82}Na_{0.115})_{\Sigma 0.935}$ $(Mg_{2.28}Al_{0.495}Fe_{0.12})_{\Sigma 2.895}$ $(Al_{1.215}Si_{2.785})O_{10}$ $[(OH)_{1.932}F_{0.068}]_{\Sigma 2}$. Although the structural formula shows a small deficiency (0.065 atoms) at the interlayer site, this is believed to be related to vacancies rather than H_2O or H_3O^+. The analysis (Pryce 1973) showed no H_2O^- (evolved H_2O at lower temperatures), and all H_2O is reported as H_2O^+ (evolved H_2O at higher temperatures, presumably relating to hydroxyl groups).

Most crystals show diffuse streaking in Buerger precession photographs, indicating stacking disorder and multiple twinning effects. However, after about 150 crystals were examined, a suitable crystal, measuring $0.4 \times 0.2 \times 0.1$ mm, was found for further study. This crystal was found to be free of diffuse streaking, but did show extra reflections unrelated to the phlogopite phase. The presence of $h + k = 2n$ reflections in precession photographs confirmed a *C*-centered unit cell, and space group *C2/m* was assumed on the basis of the findings of Hazen & Burnham (1972).

The Fe-rich phlogopite studied is from the Silver Crater mine, near Bancroft, Ontario (Canadian Museum of Nature #MOC2661). The original sample was a chemically homogeneous, euhedral single crystal measuring 4×5 cm and about 1 cm thick. We examined an unheated fragment and a cleavage sample (approximately 0.4 mm thick) heated in air to a recorded temperature of 904°C for 24 hours. The composition (Rancourt *et al.* 1993) of the unheated sample is $(K_{1.85}Na_{0.16})$ $(Mg_{3.14}Fe^{2+}_{2.13}Fe^{3+}_{0.21}Ti_{0.21}$ $Mn_{0.12}\square_{0.19})$ $(Si_{5.94}Al_{2.01}Ti_{0.05})$ O_{20} $[OH_{2.10}F_{1.88}Cl_{0.02}]$. On the basis

of an electron-microprobe and Mössbauer study, the composition of the heat-treated sample changed by a loss of Na from 0.16 to 0.08, the amount of iron oxidation (to $Fe^{2+}_{0.37}Fe^{3+}_{1.97}$), and the amount of presumed loss of hydrogen for charge compensation. No Fe^{3+} was observed to be tetrahedrally coordinated according to Mössbauer spectra, and the F content did not change between the untreated and heat-treated samples.

A rectangular fragment approximately 0.5 × 0.3 × 0.025 mm was cut from the untreated material, and an irregular fragment about 0.3 × 0.4 × 0.015 mm was obtained from the heat-treated sample. Both crystals showed sharp reflections, with little mosaic spread. Examination of zero- and upper-level photographs indicated the presence of reflections of type $h + k = 2n$, which define a *C*-centered cell. On the basis of an apparent 2-fold and *m* plane and cell geometry, space group *C2/m* was assumed for each crystal. This is consistent with the 1*M* polytype.

In situ heating, data collection, and refinement of end-member phlogopite

The phlogopite crystal was inserted into a glass capillary and another smaller capillary was then introduced into the first so that the crystal was wedged against the inner walls of the outer tube. The inner capillary was prevented from moving by fusing one end in a torch while evacuating the assembly. The furnace (Brown *et al.* 1973) was calibrated on the Picker four-circle diffractometer using the technique described in Guggenheim *et al.* (1987) using crystals of phenolphthalein, $NaNO_3$, $Ca(NO_3)_2$, and $MgCl_2$ with known melting points of 261°, 307°, 561°, and 708°C, respectively. Single-crystal data were collected by using a Picker four-circle X-ray diffractometer (Mo*K*α radiation, 0.71073 Å), controlled by programs written by D.W. Bennett and modified by D. Schiferl (Bennett and Schiferl, unpublished programs, 1994).

Unit-cell parameters (Table 1) were measured at temperatures of 20, 150, 200, 250, 300, 350, 400, 450, 500, 550, and 600°C, using least-squares refinement of 160 medium-angle reflections (20 reflections, each measured from eight octants). In addition, complete structural refinements were performed at temperatures of 20°, 300°, 450°, and 600°C. Each time the temperature setting was changed, the system was allowed to equilibrate for at least 3 hours before unit-cell measurements were taken, and 12 hours before the collection of structure data resumed.

TABLE 1. UNIT-CELL DIMENSIONS OF PHLOGOPITE AS A FUNCTION OF TEMPERATURE

T (°C)	*a* (Å)	*b* (Å)	*c* (Å)	β (°)	*V* (Å³)
20	5.3030(4)	9.1805(6)	10.2483(7)	100.05(6)	491.27(6)
150	5.3076(6)	9.1868(9)	10.261(1)	100.052(9)	492.62(9)
200	5.3115(6)	9.1932(9)	10.2666(7)	100.049(7)	493.62(8)
250	5.3156(7)	9.1998(9)	10.279(1)	100.043(9)	494.96(9)
300	5.3193(7)	9.207(1)	10.286(1)	100.042(9)	496.0(1)
350	5.3230(6)	9.2132(8)	10.294(1)	100.040(9)	497.11(9)
400	5.3273(6)	9.2215(7)	10.3041(9)	100.044(8)	498.44(8)
450	5.3331(7)	9.2316(9)	10.3159(8)	100.004(8)	500.20(9)
500	5.3371(5)	9.2396(8)	10.327(1)	99.984(8)	501.55(8)
550	5.3399(8)	9.245(1)	10.336(1)	99.96(1)	502.5(1)
600	5.342(3)	9.238(4)	10.357(5)	99.99(1)	503.4(4)

For the structural refinements, data from four octants of the limiting sphere were collected, ranging from $-7 \leq h \leq 7$, $0 \leq k \leq 12$, and $-14 \leq l \leq 14$. The scan rate used was 1°/minute, with a scan-window width of 2.0° (adjusted for dispersion as 2θ changed), and background time of one half the data-collection time for that reflection. The scanning mode was 2θ:θ, and three reflections were chosen as standards and monitored every 200 minutes as an ongoing test for stability of both the electronics and the crystal.

The structure data were refined using the program SDPWIN (Frenz 1995). Of a total of 1667 reflections collected at 20°C, 422 were deleted because of interference of the X-ray beam by the furnace. When averaged for the effects of symmetry, the remaining 1245 reflections resulted in 754 unique nonzero reflections. The higher-temperature datasets resulted in 732 observations at 300°C, 731 observations at 450°C, and 852 observations at 600°C. Initial scattering factor curves for mixed-occupancy sites were obtained using the method of Sales (1987) and initial values from Cromer & Mann (1968). In SDPWIN, the scale factor and atomic position parameters were allowed to vary in space group *C2/m*. In early refinement-cycles, initial scattering-factors were tested by allowing site-occupancy factors to vary. Scattering factors were adjusted until occupancy factors approached the chemical data, then site-occupancy factors were fixed, and isotropic temperature and anisotropic temperature parameters were allowed to vary (73 variables). Final *R* values are: room temperature, $R = 0.097$, $wR = 0.102$; 300°C, $R = 0.128$, $wR = 0.137$; 450°C, $R = 0.119$, $wR = 0.129$, and 600°C, $R = 0.069$, $wR = 0.096$.

Data collection and refinement of Fe-rich phlogopite

Datasets for the untreated and the heat-treated samples were obtained in similar ways, so that meaningful comparisons could be made. Cell parameters were refined from 20 (untreated) and 15 (heat-treated) high-angle reflections, each measured in eight octants, to produce 160 (untreated) and 120 (heat-treated) independent measurements to yield (untreated): *a* 5.3346(7), *b* 9.2417(8), *c* 10.182(2) Å, β 100.26(1)°, and (heat treated), *a* 5.3099(5), *b* 9.185(1), *c* 10.093(2) Å, β 100.07(1)°. Approximately 1,800 reflections were measured for each sample over the 2θ range 4–60° in the 2θ:θ scan mode at a scan rate of 1°/min, a 10 s background time, and with a 2.1° scan window for the un-

treated sample and a 2.0° scan window for the heat-treated sample. Reflections were measured in one-half of the limiting sphere, with indices varying as follows: $-7 \le h \le 7$, $0 \le k \le 12$, $-14 \le l \le 14$. Three standard reflections were measured every 200 min to check for crystal and electronic stability. If I exceeds 6σ, then reflections were considered observed, where $\sigma(I) = [CT + 0.25(t_c/t_b)^2(B_1 + B_2) + (pI)^2]^{1/2}$, and CT is the total integrated count in time t_c, B_1 and B_2 are the background counts in time t_b, and p (the estimate of the standard error) is equal to 0.03.

After Lorentz-polarization corrections, absorption corrections were made empirically based on reflection measurements at different azimuthal angles at psi increments of 30° and from measurements of equivalent reflections using program XEMP (Sheldrick 1990). Approximately 380 measurements were made for each crystal, and a "pseudo-ellipsoid" correction was used. Reflections were symmetry-averaged according to Laue group 2/*m*. This resulted in 700 (untreated) and 646 (heat-treated) unique nonzero reflections. Twelve reflections were removed from each data set near the final stages of refinement according to the equation $|F_o-F_c| > 2[\sigma(F_o-F_c)^2/M-N]^{1/2}$, where M represents the number of reflections, and N stands for the number of parameters.

The crystallographic least-squares program SHELXTL PLUS (Sheldrick 1990) was used, with initial atomic coordinates taken from Hazen & Burnham (1972). Scattering factor curves in an exponential form were calculated using the method of Sales (1987), with initial values from Cromer & Mann (1968). All atoms were considered half-ionized. Reflections were assigned unit weights with a single scale-factor. The scale-factor was initially varied, followed by atomic coordinates, and isotropic temperature-factors in succeeding cycles. Site-occupancy factors were allowed to vary at this stage to check for variations in assigned occupancy, but adjustments were not necessary. Site occupancies, which did not significantly differ between the two refinements, were determined approximately to be $M1 = M2 = 0.54Mg + 0.41Fe + 0.03Ti = 17.2$ electrons, $T = 0.745Si + 0.255Al = 11.87$ electrons, interlayer $= 0.92K + 0.08Na = 17.88$ electrons, $OH,F = 0.45O + 0.55F = 9.27$ electrons. Site-occupancy factors were then fixed. The R factor was 0.063 and $wR = 0.064$ [where $wR = [\Sigma w(|F_o| - |F_c|)^2/\Sigma w|F_o|^2]^{1/2}$] for the untreated sample, and $R = 0.072$ and $wR = 0.081$ for the heat-treated sample. Anisotropic temperature-factors were then allowed to vary. Final R factors are $R = 0.039$ and $wR = 0.043$ for the untreated crystal and $R = 0.039$ and $wR = 0.047$ for the heat-treated sample. There were a total of 53 varied parameters.

Final atomic coordinates and thermal parameters for all structure determinations are given in Table 2, and bond lengths and angles are compared in Table 3. Structure-factor data are on deposit at the Depository of Unpublished Data, Canadian Institute for Scientific and Technical Information, National Research Council, Ottawa, Ontario K1A 0S2, Canada.

Discussion

End-member phlogopite

Room-temperature *a* and *b* axes for the White Well phlogopite are smaller than for the F-rich phlogopite (Takeda & Morosin 1975), but the *c*-axis dimension is larger owing to H^+ – interlayer K^+ repulsions, as predicted by Noda & Roy (1956). Figure 1 shows axial expansion of the White Well phlogopite compared to fluorophlogopite (Takeda & Morosin 1975). The White Well phlogopite shows an expansion rate of the *c* axis greater than the *a* or *b* axes over the 20°–600°C range. The *c* axis expansivity is $1.81 \times 10^{-5}°C^{-1}$, and 1.40 and $1.34 \times 10^{-5}°C^{-1}$ for the *a* and *b* axes (compared to fluorophlogopite: 24° to 600°C, $\alpha_a = 0.86$, $\alpha_b = 0.75$, and $\alpha_c = 1.81 \times 10^{-5}°C^{-1}$). The volume increase of the unit cell is thus dominated over all temperature intervals by expansion of the *c* axis.

Although errors in temperature calibration of the furnace are probably near 3%, actual deviations in temperature are generally much higher. Four-circle diffractometers must position the crystal (and furnace) by ±180° within a plane nearly perpendicular to the incident X-ray beam (*i.e.*, ψ circle) to obtain the required data for cell-parameter refinement. The furnace varies considerably in orientation, convection affects the crystal's temperature, and thus the recorded temperature is an average value. Considering these effects, we do not observe any significant deviation from a straight line for our cell-parameter plots. However, we have treated the data from Takeda & Morosin (1975) with a break in slope near 400°C, as indicated in the original paper.

The lateral expansion of the octahedral sheet determines how much tetrahedral rotation (Table 4) is required to accommodate the linkage between octahedral and tetrahedral sheets. Fluorophlogopite (Takeda & Morosin 1975) has the smaller misfit and displays less tetrahedral rotation at all temperatures than phlogopite. The expansion in the octahedral sheet results in the tetrahedron rotation angle, α, decreasing with increasing temperature, from 11.3° at 20°C to 6.7° at 600°C in phlogopite and from 6.4° at 24°C to 2.7° at 700°C in fluorophlogopite (Fig. 2). Because of the lack of data at intermediate temperatures, the fluorophlogopite curve is drawn as a straight line in Figure 2.

An ideal octahedron has an angle, Ψ, of 54.73°, where this angle (Table 4) is measured between the body diagonal and the normal to the top plane. If this angle is greater than the ideal value, the octahedron is flattened, and octahedral thickness is reduced. The Mg octahedra (*M*1, *M*2) in phlogopite are flattened and essentially fixed in shape with increasing temperature, with *M*1 octahedra decreasing in Ψ value by 0.22° (59.12° to

TABLE 2a. POSITIONAL COORDINATES AND DISPLACEMENT PARAMETERS FOR PHLOGOPITE

Atom	x	y	z	U(1,1)	U(2,2)	U(3,3)	U(1,2)	U(1,3)	U(2,3)
					20°C				
K	0.0000	0.5000	0.0000	0.3409(19)	0.0355(22)	0.0381(20)	0.0000	0.0056(17)	0.0000
M1	0.0000	0.0000	0.5000	0.0033(15)	0.0022(17)	0.0158(18)	0.0000	0.0022(14)	0.0000
M2	0.0000	0.3318(3)	0.5000	0.0007(10)	0.0025(10)	0.0145(12)	0.0000	0.0006(9)	0.0000
T	0.0759(6)	0.1668(2)	0.2282(2)	0.0051(6)	0.0060(7)	0.0159(7)	0.0000(6)	0.0021(6)	0.0001(7)
O1	-0.0001(15)	0.0000	0.1713(8)	0.0165(3)	0.0152(3)	0.0215(30)	0.0000	0.0019(2)	0.0000
O2	0.3364(9)	0.2214(6)	0.1714(5)	0.0107(18)	0.0177(24)	0.0254(23)	0.0063(19)	0.0060(17)	0.0042(21)
O3	0.1317(9)	0.1677(5)	0.3925(5)	0.0061(17)	0.0059(19)	0.0176(20)	0.0002(16)	0.0012(16)	0.0003(18)
OH	0.1309(13)	0.5000	0.3985(7)	0.0166(27)	0.0175(30)	0.0292(31)	0.0000	0.0020(25)	0.0000
					300°C				
K	0.0000	0.5000	0.0000	0.0705(44)	0.0792(52)	0.0535(36)	0.0000	0.0067(34)	0.0000
M1	0.0000	0.0000	0.5000	0.0154(24)	0.0296(32)	0.0208(26)	0.0000	0.0021(22)	0.0000
M2	0.0000	0.3319(6)	0.5000	0.0151(16)	0.0306(22)	0.0196(17)	0.0000	0.0008(15)	0.0000
T	0.0769(5)	0.1669(3)	0.2290(3)	0.0200(10)	0.0316(13)	0.0196(10)	0.0003(11)	0.0014(9)	-0.0004(11)
O1	0.0096(23)	0.0000	0.1796(11)	0.0391(54)	0.0304(51)	0.0324(50)	0.0000	0.0041(45)	0.0000
O2	0.3318(14)	0.2251(10)	0.1730(7)	0.0311(32)	0.0413(41)	0.0332(33)	-0.000(3)	0.0071(28)	-0.009(3)
O3	0.1314(12)	0.1675(8)	0.3934(6)	0.0220(27)	0.0332(34)	0.0213(27)	0.0032(29)	0.0014(24)	0.000(3)
OH	0.1311(19)	0.5000	0.3977(10)	0.0331(44)	0.0451(53)	0.0375(46)	0.0000	0.0016(39)	0.0000
					450°c				
K	0.0000	0.5000	0.0000	0.0865(52)	0.0923(60)	0.0689(44)	0.0000	0.0133(40)	0.0000
M1	0.0000	0.0000	0.5000	0.0159(22)	0.0300(30)	0.0258(26)	0.0000	0.0043(20)	0.0000
M2	0.0000	0.3317(5)	0.5000	0.0157(15)	0.0302(21)	0.0239(17)	0.0000	0.0018(13)	0.0000
T	0.0768(5)	0.1668(3)	0.2296(2)	0.0206(9)	0.0308(12)	0.0232(10)	0.0003(11)	0.0028(8)	-0.0001(10)
O1	0.0179(22)	0.0000	0.1727(11)	0.0457(56)	0.0291(48)	0.0382(52)	0.0000	0.0012(4)	0.0000
O2	0.3373(13	0.2289(9)	0.1733(7)	0.0319(31)	0.0429(40)	0.0398(34)	-0.0090(32)	0.0089(27)	-0.0078(33)
O3	0.1315(12)	0.1673(8)	0.3933(6)	0.0227(25)	0.0350(33)	0.0255(27)	0.0018(28)	0.0022(22)	-0.0011(28)
OH	0.1320(18)	0.5000	0.3978(10)	0.0359(41)	0.0473(52)	0.0461(48)	0.0000	0.0046(39)	0.0000
					600°c				
K	0.0000	0.5000	0.0000	0.0918(43)	0.1054(53)	0.0864(42)	0.0000	0.0154(35)	0.0000
M1	0.0000	0.0000	0.5000	0.0151(19)	0.0212(23)	0.0333(25)	0.0000	0.0067(18)	0.0000
M2	0.0000	0.3317(4)	0.5000	0.0131(12)	0.0207(16)	0.0312(15)	0.0000	0.0045(11)	0.0000
T	0.0711(3)	0.1667(2)	0.2302(2)	0.0162(7)	0.0230(9)	0.0316(9)	-0.0004(10)	0.0054(7)	0.0003(11)
O1	0.0238(16)	0.0000	0.1731(9)	0.0449(44)	0.0223(38)	0.0452(47)	0.0000	0.0004(39)	0.0000
O2	0.3254(10)	0.2334(7)	0.1732(6)	0.0263(23)	0.0417(33)	0.0501(31)	-0.0182(24)	0.0110(22)	-0.0027(29)
O3	0.1312(9)	0.1673(6)	0.3928(5)	0.0212(20)	0.0323(27)	0.0314(24)	-0.0010(24)	0.0046(19)	-0.0013(25)
OH	0.1312(14)	0.5000	0.3976(8)	0.0367(35)	0.0502(46)	0.0600(45)	0.0000	0.0076(34)	0.0000

The form of the anisotropic displacement parameter is:

$$\exp[-2\pi^2(h^2a^{*2}U(1,1) + k^2b^{*2}U(2,2)+l^2c^{*2}U(3,3)+2hka^*b^*U(1,2)+2hla^*c^*U(1,3)+2klb^*c^*U(2,3)]$$

TABLE 2b. POSITIONAL COORDINATES AND DISPLACEMENT PARAMETERS FOR UNTREATED AND HEAT-TREATED Fe-RICH PHLOGOPITE

Site	x	y	z	U_{eq}	U_{11}	U_{22}	U_{33}	U_{12}	U_{13}	U_{23}
					Untreated					
K	0.0	0.5	0.0	0.0482(8)	0.043(1)	0.046(1)	0.055(1)	0.0	0.009(1)	0.0
M1	0.0	0.0	0.5	0.0205(4)	0.0165(6)	0.0181(7)	0.0272(7)	0.0	0.0053(5)	0.0
M2	0.0	0.3333(1)	0.5	0.0228(3)	0.0174(4)	0.0225(5)	0.0286(5)	0.0	0.0042(4)	0.0
T	0.0744(2)	0.1666(1)	0.2252(1)	0.0203(3)	0.0169(4)	0.0194(4)	0.0247(5)	0.0000(4)	0.0037(3)	0.0001(4)
O1	0.0330(8)	0.0	0.1668(4)	0.029(1)	0.035(2)	0.023(2)	0.026(2)	0.0	0.001(2)	0.0
O2	0.3154(5)	0.2391(3)	0.1670(3)	0.0308(8)	0.026(1)	0.036(2)	0.031(1)	-0.007(1)	0.007(1)	-0.003(1)
O3	0.1307(5)	0.1668(3)	0.3893(3)	0.0222(7)	0.020(1)	0.022(1)	0.025(1)	0.0000(9)	0.0042(9)	0.000(1)
O4	0.1299(6)	0.5	0.3958(4)	0.027(1)	0.022(2)	0.025(2)	0.033(2)	0.0	0.005(1)	0.0
					Heat-treated					
K	0.0	0.5	0.0	0.0327(7)	0.031(1)	0.029(1)	0.039(1)	0.0	0.007(1)	0.0
M1	0.0	0.0	0.5	0.0181(5)	0.0144(9)	0.0132(8)	0.028(1)	0.0	0.0058(7)	0.0
M2	0.0	0.3420(1)	0.5	0.0145(3)	0.0086(5)	0.0131(6)	0.0216(6)	0.0	0.0022(4)	0.0
T	0.0734(2)	0.1674(1)	0.2232(1)	0.0112(3)	0.0081(5)	0.0078(5)	0.0177(5)	0.0000(4)	0.0025(4)	0.0001(4)
O1	0.0310(9)	0.0	0.1661(5)	0.020(1)	0.028(2)	0.011(2)	0.021(2)	0.0	0.003(2)	0.0
O2	0.3155(6)	0.2380(4)	0.1645(3)	0.0216(9)	0.016(1)	0.025(2)	0.024(2)	-0.005(1)	0.005(1)	-0.002(1)
O3	0.1295(5)	0.1694(3)	0.3896(3)	0.0128(7)	0.010(1)	0.011(1)	0.017(1)	0.001(2)	0.002(1)	0.001(1)
O4	0.1359(8)	0.5	0.4010(4)	0.016(1)	0.014(2)	0.012(2)	0.023(2)	0.0	0.004(1)	0.0

58.90° at 600°C) and Ψ for *M*2 decreasing by 0.12° (58.90° *versus* 58.78°). Thus, the octahedra are expanding without significantly changing shape. In contrast, the average Ψ angle for fluorophlogopite changes by –0.74% over the same temperature interval, with a rela-

TABLE 3a. SELECTED INTERATOMIC DISTANCES FOR PHLOGOPITE

	20°C	300°C	450°C	600°C
		Tetrahedral site		
T – O1	1.663(4)	1.663(5)	1.658(5)	1.653(4)
– O2	1.658(5)	1.661(8)	1.624(7)	1.629(6)
– O2[1]	1.667(5)	1.652(7)	1.696(7)	1.689(5)
– O3	1.658(5)	1.665(7)	1.663(6)	1.659(6)
Mean *T* – O	1.662	1.660	1.660	1.658
Basal–basal				
O1 – O2	2.705(7)	2.703(10)	2.714(10)	2.692(7)
– O2[1]	2.701(6)	2.688(10)	2.682(9)	2.681(7)
O2– O2[1]	2.703(6)	2.699(9)	2.695(8)	2.689(6)
Apical–basal				
O1 – O3	2.729(8)	2.736(11)	2.730(11)	2.728(9)
O2 – O3	2.723(7)	2.720(10)	2.747(9)	2.728(8)
O2[1] – O3	2.718(7)	2.720(9)	2.701(9)	2.719(8)
Mean O – O	2.713	2.711	2.712	2.706
		Octahedral sites		
*M*1– O3 [×4]	2.083(5)	2.082(7)	2.087(7)	2.093(5)
– OH [×2]	2.050(6)	2.059(9)	2.060(9)	2.069(7)
Mean *M* – O	2.072	2.074	2.078	2.085
O – O shared (*M*1 and *M*2)				
O3 – O3 [×2]	2.807(7)	2.799(8)	2.808(8)	2.824(6)
– OH [×4]	2.757(7)	2.765(10)	2.771(10)	2.785(8)
O – O unshared (triads)				
O3 – O3 [×2]	3.079(7)	3.084(25)	3.089(10)	3.091(8)
– OH [×4]	3.080(6)	3.083(9)	3.087(9)	3.094(7)
Mean O – O	2.927	2.810	2.936	2.946
*M*2 – O3 [×2]	2.059(5)	2.061(8)	2.068(8)	2.074(6)
– O3[1] [×2]	2.068(4)	2.073(6)	2.079(6)	2.087(4)
– OH [×2]	2.050(5)	2.060(8)	2.069(7)	2.072(6)
Mean *M* – O	2.059	2.065	2.072	2.078
O – O shared (*M*1 and *M*2)				
O3 – O3	2.807(7)	2.799(8)	2.808(8)	2.824(6)
– OH [×2]	2.757(7)	2.765(10)	2.771(10)	2.785(8)
O – O shared (*M*2 and *M*2)				
O3 – O3 [×2]	2.784(7)	2.783(9)	2.795(9)	2.810(7)
OH – OH	2.695(9)	2.720(13)	2.731(13)	2.738(10)
O – O unshared (triads)				
O3 – O3 [×2]	3.052(6)	3.063(8)	3.073(8)	3.077(6)
– OH [×2]	3.051(5)	3.062(7)	3.072(7)	3.074(6)
– OH[1] [×2]	3.054(6)	3.067(9)	3.077(9)	3.079(7)
Mean O – O	2.908	2.917	2.926	2.934
		Interlayer–inner		
K – O1 [×2]	2.913(7)	2.966(11)	3.016(11)	3.050(8)
– O2 [×4]	2.916(5)	2.969(8)	2.992(8)	3.052(6)
Mean	2.915	2.968	3.000	3.051
		Interlayer–outer		
K – O1 [×2]	3.427(7)	3.395(11)	3.373(10)	3.357(8)
– O2 [×4]	3.423(5)	3.405(8)	3.403(8)	3.350(6)
Mean	3.424	3.402	3.393	3.352

[1] atom position derived by one or more symmetry transformations. All distances are expressed in Å.

TABLE 3b. INTERATOMIC DISTANCES FOR UNTREATED AND HEAT-TREATED Fe-RICH PHLOGOPITE

Bond	Distance (Å) Untreated	Heated	Linkage	Angle (°) Untreated	Heated
			Tetrahedra		
			basal–*T*–basal		
T – O1	1.651(2)	1.644(2)	O1–*T*–O2	108.2(2)	108.1(2)
– O2	1.651(3)	1.642(3)	–*T*–O2'	108.3(2)	108.3(2)
– O2'	1.652(3)	1.644(3)	O2–*T*–O2'	108.2(1)	108.5(2)
– O3	1.644(3)	1.654(3)	apical–*T*–basal		
Mean	1.650	1.646	O1–*T*–O3	110.8(2)	110.8(2)
			O2–*T*–O3	110.6(1)	110.4(1)
basal–basal			O2'–*T*–O3	110.7(1)	110.6(1)
O1 – O2	2.674(3)	2.659(4)	Mean	109.5	109.5
O1 – O2'	2.676(3)	2.664(4)			
O2 – O2'	2.675(3)	2.664(4)			
apical–basal					
O1 – O3	2.713(4)	2.715(5)			
O2 – O3	2.708(4)	2.705(4)			
O2' – O3	2.712(4)	2.709(4)			
Mean	2.693	2.686			
T – *T*	3.079(1)	3.058(1)			
T – *T*"	3.081(1)	3.075(1)			
Mean	3.080	3.067			
			*M*1 Octahedra		
*M*1 – O3 [×4]	2.101(3)	2.098(3)	O3–*M*1–O3' [×2]	85.6(1)	84.3(1)
– OH [×2]	2.068(3)	2.015(4)	–*M*1–O3' [×2]	94.4(1)	95.7(1)
Mean	2.090	2.070	–*M*1–OH [×4]	84.1(1)	83.6(1)
			–*M*1–OH [×4]	95.9(1)	96.4(1)
O – O shared (*M*1 and *M*2)			Mean	90.0	90.0
O3 – O3 [×2]	2.854(4)	2.816(4)			
– OH [×4]	2.793(4)	2.742(4)			
O – O unshared (triads)					
O3 – O3 [×2]	3.083(4)	3.112(4)			
– OH [×4]	3.095(3)	3.067(4)			
Mean	2.952	2.924			
			*M*2 Octahedra		
*M*2 – O3 [×2]	2.099(3)	2.120(3)	O3–*M*2–O3	85.7(1)	83.2(1)
– O3' [×2]	2.088(2)	2.087(2)	–*M*2–O3 [×2]	85.3(1)	83.2(1)
– OH [×2]	2.059(2)	1.969(3)	–*M*2–O3 [×2]	94.7(1)	92.5(1)
Mean	2.082	2.059	–*M*2–OH [×2]	84.7(1)	85.0(1)
			–*M*2–OH [×2]	95.4(1)	99.3(1)
O – O shared (*M*1 and *M*2)			–*M*2–OH [×2]	95.6(1)	95.9(1)
O3 – O3	2.854(4)	2.816(4)	OH–*M*2–OH	83.2(1)	85.1(1)
– OH [×2]	2.793(4)	2.742(4)	Mean	90.0	90.0
O – O shared (*M*2 and *M*2)					
O3 – O3 [×2]	2.836(4)	2.793(4)			
OH – OH	2.733(5)	2.662(5)			
O – O unshared (triads)					
O3 – O3 [×2]	3.079(3)	3.040(3)			
– OH [×2]	3.068(3)	3.091(4)			
O3' – OH [×2]	3.080(3)	3.039(3)			
Mean	2.942	2.907			
			Interlayer		
K – O1 [×2]	3.041(4)	3.018(4)			
– O2 [×4]	3.056(3)	3.011(3)			
Mean (inner)	3.051	3.013			
K – O1 [×2]	3.255(4)	3.236(4)			
– O2 [×4]	3.243(3)	3.222(3)			
Mean (outer)	3.247	3.227			

Bond and angle multiplicities are given in brackets.
[1] atom position derived by one or more symmetry transformations.

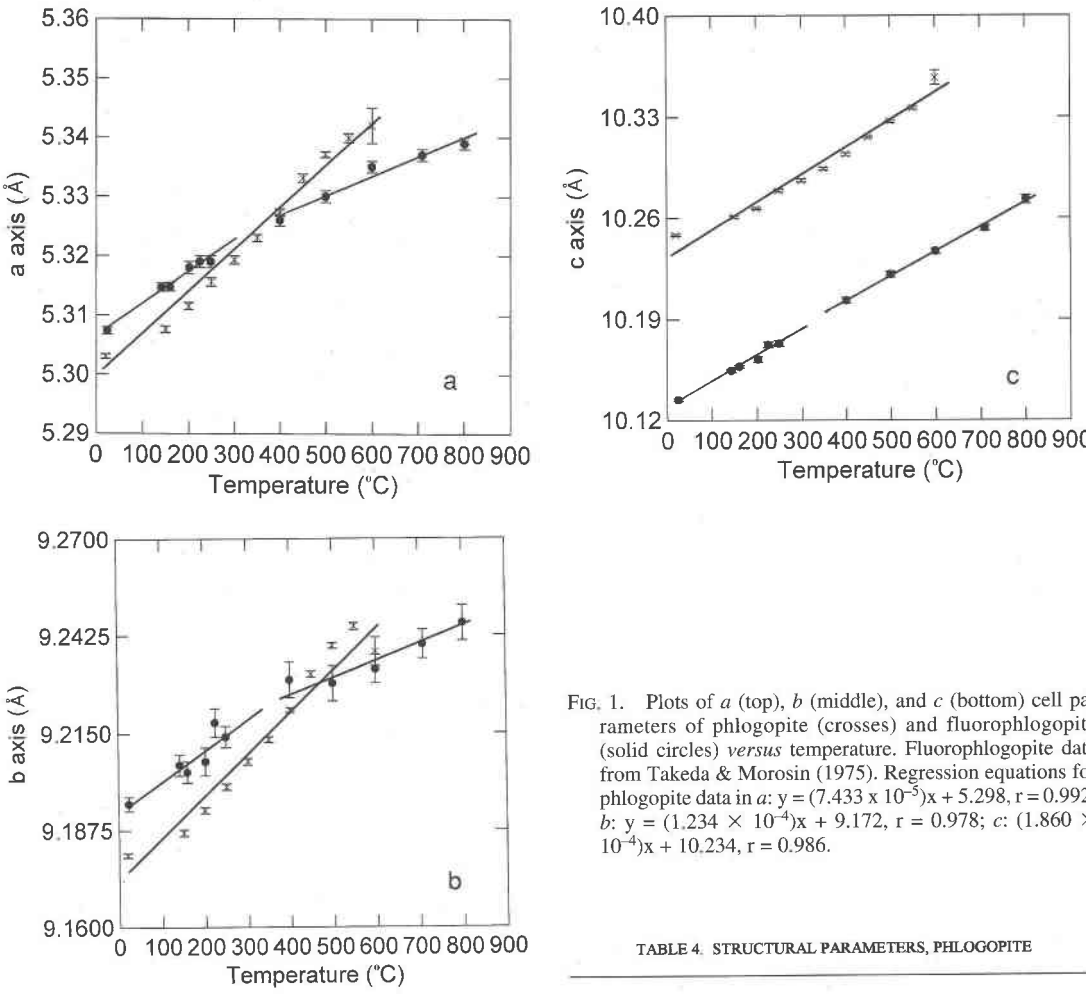

FIG. 1. Plots of *a* (top), *b* (middle), and *c* (bottom) cell parameters of phlogopite (crosses) and fluorophlogopite (solid circles) *versus* temperature. Fluorophlogopite data from Takeda & Morosin (1975). Regression equations for phlogopite data in *a*: $y = (7.433 \times 10^{-5})x + 5.298$, $r = 0.992$; *b*: $y = (1.234 \times 10^{-4})x + 9.172$, $r = 0.978$; *c*: $(1.860 \times 10^{-4})x + 10.234$, $r = 0.986$.

tive elongation of octahedra parallel to (001)*. Since the rate of octahedron expansion in fluorophlogopite is similar to that in end-member phlogopite (Fig. 3), the octahedral sheet thickens in fluorophlogopite at the expense of lateral expansion when compared to end-member phlogopite. Therefore, lateral expansion along the *a* and *b* axes is less in the F-rich structure (Fig. 1). The thickness of the octahedral sheet in the F-rich structure, however, expands much faster than does the octahedron thickness of the OH-rich structure (Fig. 4).

The interlayer K-octahedron in phlogopite, using nearest-neighbor anions only to define the polyhedron, is elongate parallel to (001)*, whereas the K-site in the F-rich sample (24°C: 56.13°; 700°C: 56.52°) is compressed parallel to (001)* (Table 4). This relationship, as well as a smaller interlayer separation (Fig. 5), exists because of the attractive forces between K^+ and F^- (*versus* repulsions occurring between K and H in the hy-

TABLE 4. STRUCTURAL PARAMETERS, PHLOGOPITE

Parameter	Phlogopite				Fe-rich Phlogopite	
	20°C	300°C	450°C	600°C	Unheated	Heated
α_{tet}(°)*	11.3(3)	9.6(4)	8.7(4)	6.7(3)	4.3(1)	4.7(2)
β_{ideal}(°)**	99.93	99.93	99.92	99.90	99.87	100.10
ψ(°)†						
Interlayer	53.62	53.99	54.08	54.62	56.77	57.03
*M*1	59.12	59.09	59.04	58.90	58.66	59.21
*M*2	58.90	58.94	58.94	58.78	58.53	59.03
Sheet thickness (Å)						
Tetrahedral	2.253	2.251	2.256	2.256	2.249	2.270
Octahedral	2.127	2.131	2.138	2.154	2.174	2.119
Interlayer separation (Å)	3.458	3.490	3.520	3.533	3.344	3.279
τ(°)§	110.18	110.17	110.25	110.55	109.5	110.6

*α_{tet} = (½120° – mean O_{basal}–O_{basal}–O_{basal} angle|).
**β_{ideal} = [180° – $\cos^{-1}(a/3c)$].
† cos ψ = (octahedral thickness)/[2(mean *M*–O,OH distance)]. The ideal value is 54.73°.
§ τ = O_{apical}–*T*–O_{basal} angle.

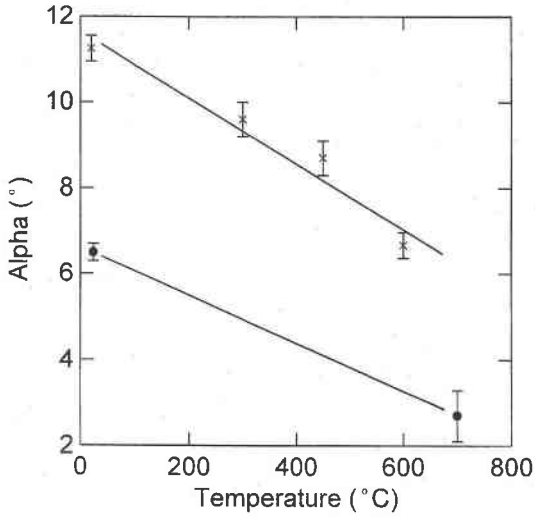

FIG. 2. Comparison of tetrahedral rotation angle, α, *versus* temperature for phlogopite (crosses) and fluorophlogopite (solid circles). A linear representation for the rotation angle *versus* temperature for fluorophlogopite is given owing to lack of additional data.

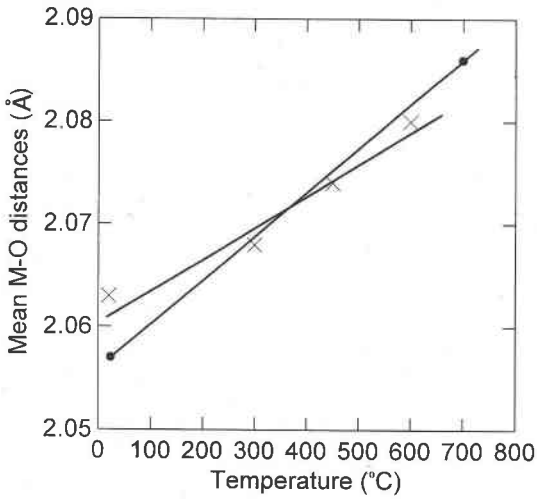

FIG. 3. Comparison of mean M–O,OH,F distances *versus* temperature for phlogopite (crosses) and fluorophlogopite (solid circles).

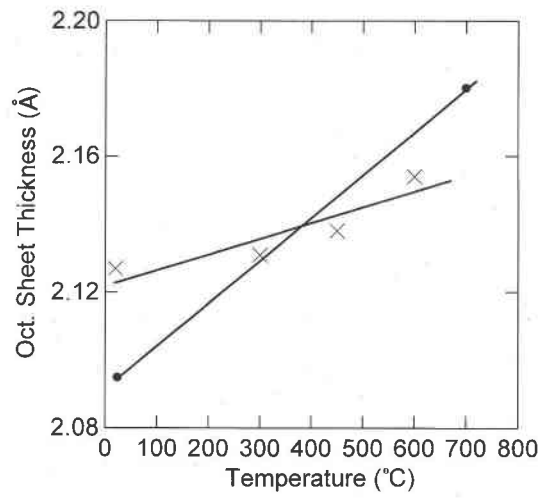

FIG. 4. Comparison of octahedral sheet thickness *versus* temperature for phlogopite (crosses) and fluorophlogopite (solid circles).

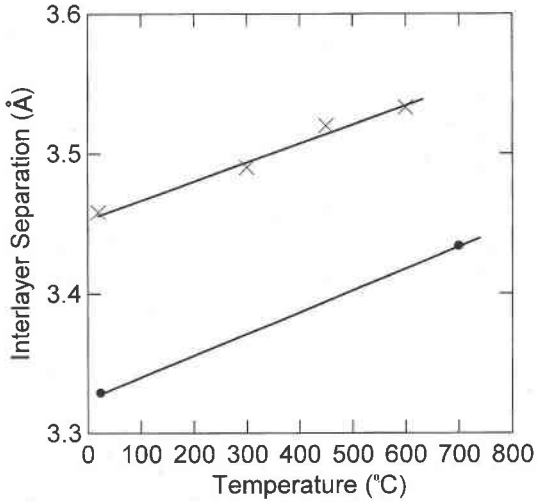

FIG. 5. Comparison of interlayer separation *versus* temperature for phlogopite (crosses) and fluorophlogopite (solid circles).

droxyl-rich sample). However, fluorophlogopite has the longest first nearest-neighbor K–O bond distances at all temperatures compared to phlogopite. In both samples, the Ψ value for the interlayer K site generally increases as temperature increases, with accompanying flattening of the interlayer K site. Thus, expansion of the upper and lower oxygen triads forming the interlayer octahedron is greater than necessary to maintain the shape of the octahedron as the interlayer separation increases.

Fe-rich phlogopite

Table 4 presents structural parameters typically used to analyze phyllosilicates. Many of the trends observed

in this study confirm the trends found by Ohta *et al.* (1982) for the oxidation–reduction experiments using argon and hydrogen (Takeda & Ross 1975), although the magnitudes are somewhat larger in our study because of the greater amounts of iron present in the phlogopite from Silver Crater. For example, like the phlogopite from Ruiz Peak examined by Ohta *et al.* (1984), we observe a reduction in cell lengths and octahedral sheet thickness in the heat-treated sample relative to the unheated sample, which may be attributed to a change in cation size from Fe^{2+} to Fe^{3+}. In addition, the interlayer separation for the untreated sample is much greater than the heat-treated sample because the interlayer K^+ cation interacts (with repulsive forces) with the H^+, thereby weakening the K–O4 bond (Ohta *et al.* 1982). Some of our results, however, differ from the earlier work.

There is no change in tetrahedral-site occupancy upon heating for the Silver Crater phlogopite, either based on the X-ray refinement or from Mössbauer results (Rancourt *et al.* 1993). In contrast, tetrahedral iron was observed (Ohta *et al.* 1982) in both oxidized phlogopite-1*M* and phlogopite-$2M_1$, although no tetrahedral iron was present in the corresponding hydrogenated phlogopite (Takeda & Ross 1975). It seems unlikely that an exchange reaction involving the tetrahedral sites would be energetically favorable owing to the strong tetrahedral bonds. It may be noteworthy that all phlogopite crystals from the Ruiz Peak lava flow are not compositionally identical (Takeda & Ross 1975), and different crystals were used for the two studies, unlike the study reported here. We observe also that the length of the heating experiments for the Silver Crater phlogopite was 24 h (at 904°C), whereas no information was given regarding the duration of the experiments (at 700°C) in the earlier studies.

The Silver Crater phlogopite shows a change in tetrahedral rotation value from $\alpha = 4.3°$ in the unheated sample to 4.7° in the heated (oxidized) sample. This is in accordance with a reduction in size of the octahedral sheet with the change in oxidation state of the iron. Thus, the tetrahedral sheet must reduce its lateral dimensions by increasing tetrahedral rotation. Although it is difficult to estimate tetrahedral rotation precisely from chemical composition alone, the approximately 5% decrease in mean octahedral-cation size produces less tetrahedral rotation than expected based on size of the octahedrally coordinated cation. McCauley & Newnham (1971) observed that the interlayer cation may have a significant effect on tetrahedral rotation, with larger cations inhibiting rotation. Alternatively, tetrahedral rotation may be inhibited also by the interlayer cation sitting deeper within the tetrahedral ring (*e.g.*, Ohta *et al.* 1982). For the oxidized Silver Crater phlogopite, where the interlayer separation is much smaller than the untreated sample due to stronger K–O4 interactions and a greater oxy-component, K partially blocks tetrahedral rotation. The trend involving the value of α differs from that of the Ruiz Peak phlogopite-1*M* (hydrogenated: 7.6°; oxidized: 7.3°); the difference is probably related to the larger amount of iron present in the Silver Crater phlogopite.

Conclusions

In this study, we compare the effect of temperature on the OH *versus* F phlogopite-1*M* structure and the "oxy" *versus* OH-rich phlogopite-1*M* structure. In phlogopite, OH-rich octahedra expand without changing shape significantly at elevated temperatures, whereas F-rich octahedra elongate approximately parallel to the *c* axis; expansion of the *a* and *b* axes of the F-rich structure is less than for OH-rich phlogopite. In the Silver Crater phlogopite, which is intermediate in F *versus* OH composition, the octahedra are flattened, with the oxidized sample showing significant flattening over the untreated sample. Owing to attractive forces between K^+ and F^-, the interlayer site is compressed approximately along *c* in F-rich phlogopite, but elongated in the same direction in the OH-rich structure relative to fluorophlogopite, although both structures exhibit general flattening of the site with increasing temperature. The interlayer site in the Silver Crater phlogopite is flattened, both in the untreated and heat-treated samples, with greater flattening in the latter sample. Unlike the previous study of phlogopite by Ohta *et al.* (1982), the Silver Crater phlogopite does not show incorporation of iron in the tetrahedral site upon oxidation.

Acknowledgements

We thank Dr. A. Bevan, Curator of Mineralogy and Meteoritics, Western Australian Museum, Perth, Western Australia, for the phlogopite sample, and Dr. D. Rancourt, Department of Physics, University of Ottawa for the samples of Fe-rich phlogopite.

References

Anderson, D.L. (1979): Chemical stratification of the mantle. *J. Geophys. Res.* **84**, 6297-6298.

Brown, G.E., Sueno, S. & Prewitt, C.T. (1973): A new single-crystal heater for the precession camera and four-circle diffractometer. *Am. Mineral.* **70**, 1169-1179.

Cromer, D.T. & Mann, J.B. (1968): X-ray scattering factors computed from numerical Hartree–Fock wave functions. *Acta Crystallogr.* **A24**, 321-324.

Frenz, B.A. (1995): *SDP for Windows*. B.A. Frenz & Associates, Inc., College Station, Texas.

Guggenheim, S., Chang, Y.-H. & Koster van Groos, A.F. (1987); Muscovite dehydroxylation: high temperature studies. *Am. Mineral.* **72**, 537-550.

HAZEN, R.M. & BURNHAM, C.W. (1973): The crystal structure of one-layer phlogopite and annite. *Am. Mineral.* **58**, 889-900.

_____, FINGER, L.W. & KO, J. (1992): Crystal chemistry of Fe-bearing anhydrous phase B: implications for transition zone mineralogy. *Am. Mineral.* **77**, 217-220.

MASON, R.A. (1992): Models of order and iron–fluorine avoidance in biotite. *Can. Mineral.* **30**, 343- 354.

MCCAULEY, J.W. & NEWNHAM, R.E. (1971): Origin and prediction of ditrigonal distortions in micas. *Am. Mineral.* **56**, 1626-1638.

NODA, T. & ROY, R. (1956): OH–F exchange in fluorine phlogopite. *Am. Mineral.* **41**, 929-932.

OHTA, T., TAKEDA, H. & TAKÉUCHI, Y. (1982): Mica polytypism: similarities in the crystal structures of 1*M* and $2M_1$ oxybiotite. *Am. Mineral.* **67**, 298-310.

PREWITT, C.T. & FINGER, L.W. (1992): Crystal chemistry of high-pressure hydrous magnesium silicates. *In* High Pressure Research: Application to Earth and Planetary Sciences (Y. Syono & M.H. Manghnani, eds.). American Geophysical Union, Washington, D.C. (269-274).

PRYCE, M.W. (1973): Low-iron cordierite in phlogopite schist from White Well, Western Australia. *Mineral. Mag.* **39**, 241-243.

RANCOURT, D.G. (1994): Mössbauer spectroscopy of minerals. II. Problem of resolving cis and trans octahedral Fe^{2+} sites. *Phys. Chem. Minerals* **21**, 250-257.

_____, PING, J.Y. & BERMAN, R.G. (1994): Mössbauer spectroscopy of minerals. III. Octahedral-site Fe^{2+} quadripole splitting distributions in layer silicates. *Phys. Chem. Minerals* **21**, 258-267.

_____, _____, BOUKILI, B. & ROBERT, J.-L. (1996): Octahedral-site Fe^{2+} quadripole splitting distributions from Mossbauer spectroscopy along the (OH,F)-annite join. *Phys. Chem. Minerals* **23**, 63-71.

_____, TUME, P. & LALONDE, A.E. (1993): Kinetics of the $(Fe^{2+} + OH^-)_{mica} \rightarrow (Fe^{3+} + O^{2+})_{mica} + H$ oxidation reaction in bulk single-crystal biotite studied by Mössbauer spectroscopy. *Phys. Chem. Minerals* **20**, 276-284.

SALES, K.D. (1987): Atomic scattering factors for mixed atom sites. *Acta Crystallogr.* **A43**, 42-44.

SHELDRICK, G.W. (1990): SHELXTL PLUS 4.0. Siemens Analytical X-ray Instruments, Inc., Madison, Wisconsin.

TAKEDA, H. & MOROSIN, B. (1975): Comparison of observed and predicted structural parameters of mica at high temperature. *Acta Crystallogr.* **B31**, 2444-2452.

_____ & ROSS, M. (1975): Mica polytypism: dissimilarities in the crystal structures of coexisting 1*M* and $2M_1$ biotite. *Am. Mineral.* **60**, 1030-1040.

Received September 24, 1998, revised manuscript accepted May 15, 1999.